A YOLOv12-based Method for Detecting Abnormal Surface Breathing Behavior of Fish in Recirculating Aquaculture Systems

Hanqiu Feng*
Capital Normal University High School, Beijing 100048, China
*Corresponding email: tyrafeng@163.com

Abstract

Current monitoring of abnormal surface breathing behavior in recirculating aquaculture systems relies primarily on manual observation, which suffers from low efficiency, subjective judgment, and inability to achieve continuous real-time detection across large-scale facilities. However, this approach often leads to missed early warning signs of hypoxia and water quality deterioration, resulting in significant economic losses from mass fish mortality events. I present a deep learning-based detection method using (You Only Look Once) YOLOv12 to automatically identify abnormal surface breathing behavior in farmed largemouth bass (Micropterus salmoides). A dataset of 13,600 images was constructed at a commercial aquaculture facility, covering day-night cycles and varying lighting conditions including natural illumination and supplementary lighting. The model was trained using the PyTorch framework with a cosine annealing learning rate schedule over 100 epochs. Specifically, our approach is valuable in two respects: (a) It achieves a precision of 84.78% and mAP@0.5 of 77.63%, effectively distinguishing abnormal surface breathing from normal swimming behavior and meeting the low false-alarm requirements of practical aquaculture scenarios. (b) It enables continuous automated monitoring that provides timely intervention opportunities, replacing labor-intensive manual inspection and reducing operational costs.

Keywords

Recirculating aquaculture system, Fish behavior recognition, Abnormal surface breathing, Deep learning, Object detection

Introduction

Aquaculture has become one of the fastest-growing food production sectors globally, playing a vital role in meeting the increasing demand for animal protein and ensuring food security. China, as the world's largest aquaculture producer, accounts for over 60% of global aquaculture output, with a total production exceeding 41 million tons annually [1]. In recent years, recirculating aquaculture systems (RAS) have emerged as a promising alternative to traditional pond and cage culture methods, offering advantages such as high stocking density, controllable environmental conditions, efficient water utilization, and reduced environmental impact [2,3]. RAS technology enables year-round fish production independent of external climate conditions, making it increasingly attractive for intensive commercial aquaculture operations.

However, the high-density culture characteristic of RAS presents significant challenges for fish health management and welfare monitoring. The enclosed environment and elevated stocking densities substantially increase the risk of hypoxia events, which occur when dissolved oxygen levels fall below critical thresholds [4]. Fish respond to hypoxic conditions through a well-documented behavioral adaptation known as ASR, where individuals swim to the air-water interface to ventilate their gills with oxygen-rich surface water. This abnormal surface breathing behavior serves as an early warning indicator of deteriorating water quality and impending oxygen depletion. If left undetected, hypoxia can rapidly escalate into mass mortality events, causing substantial economic losses to aquaculture operations [5-7].

Current monitoring practices in RAS facilities rely predominantly on manual observation by farm personnel, which suffers from inherent limitations including subjective judgment, delayed response times, and the inability to achieve continuous real-time surveillance across large-scale operations [8]. Traditional approaches to detecting fish hypoxia have utilized water quality sensors to monitor dissolved oxygen levels. However, these methods provide only indirect assessments and may not accurately reflect the actual physiological stress experienced by the fish population [9]. Consequently, there is an urgent need for automated, vision-based monitoring systems capable of directly detecting abnormal fish behaviors in real-time.

The rapid advancement of deep learning technologies has opened new possibilities for intelligent aquaculture monitoring. Convolutional neural networks (CNNs), particularly object detection algorithms, have demonstrated remarkable success in recognizing and localizing targets in complex visual environments [10]. Among various deep learning architectures, the You Only Look Once (YOLO) series has gained widespread adoption due to its exceptional balance between detection accuracy and inference speed, making it well-suited for real-time applications [11]. The YOLO framework has undergone continuous evolution, with each iteration introducing architectural improvements to enhance performance. Recent versions including YOLOv5, YOLOv7, and YOLOv8 have been successfully applied to aquaculture scenarios, including underwater fish detection, feeding behavior analysis, and species classification [12-14].

YOLOv12, the latest advancement in this series, shifts from traditional CNN-based architecture to an attention-centric design [15]. YOLOv12 introduces several key innovations including the Area Attention (A2) module for efficient large receptive field processing, Residual Efficient Layer Aggregation Networks (R-ELAN) for enhanced feature aggregation, and architectural optimizations incorporating Flash Attention to reduce memory overhead. These improvements enable YOLOv12 to achieve state-of-the-art detection accuracy while maintaining competitive inference speeds, surpassing previous YOLO versions across multiple benchmark datasets [16].

Despite these technological advances, research specifically targeting the automated detection of abnormal surface breathing behavior in RAS environments remains limited. Most existing studies on fish behavior recognition have focused on laboratory conditions with clear water and low fish density, which may not accurately reflect the challenges encountered in commercial aquaculture settings characterized by turbid water, high stocking densities, and variable lighting conditions [17]. Furthermore, while hypoxia detection has received considerable attention, the direct visual identification of surface breathing behavior as a diagnostic indicator has been relatively unexplored. This study aims to address these gaps by developing a YOLOv12-based detection system for recognizing abnormal surface breathing behavior in farmed largemouth bass (Micropterus salmoides) under commercial RAS conditions. The main contributions of this work are as follows: (1) construction of a comprehensive dataset comprising 13,600 annotated images covering diverse lighting conditions and time periods; (2) implementation and optimization of the YOLOv12 model for detecting abnormal surface breathing behavior; (3) systematic evaluation of model performance under practical aquaculture monitoring scenarios. The proposed approach provides a technical foundation for intelligent early warning systems in precision aquaculture management.

Materials and methods

Study site and experimental animals

The experiment was conducted at a commercial recirculating aquaculture facility located in Chongqing, China. Largemouth bass (Micropterus salmoides), a species widely cultured in China due to its high market value and adaptability to intensive farming conditions, was selected as the experimental subject. As shown in Figure 1, the fish were maintained in cylindrical fiberglass tanks with a diameter of 4 meters and a water depth of 1.2 meters, ensuring uniform rearing conditions throughout the experimental period.

The RAS was equipped with mechanical filtration, biological filtration, UV sterilization, and oxygenation units to maintain optimal water quality. Water temperature was maintained at 20±1°C, and dissolved oxygen concentration was stabilized at 8.0±0.5 mg/L under normal operating conditions. Fish were fed a commercial pelleted diet twice daily at 08:00 and 18:00, with a feeding rate of approximately 1% of body weight per day. The consistent environmental conditions and standardized husbandry practices ensured that any observed surface breathing behavior could be attributed to environmental stressors rather than nutritional or health-related factors.

Image acquisition system

A surveillance-grade camera system was deployed for continuous image acquisition. A Hikvision network camera (model DS-2CD3T56DWD-I5) with 5-megapixel resolution was mounted 1.8 meters above the water surface, positioned at a top-down angle to provide comprehensive coverage of the entire tank area. This overhead perspective minimized occlusion between fish and enabled clear visualization of surface breathing behavior occurring at the air-water interface.

The camera was configured to capture images at a resolution of 1920×1080 pixels with automatic exposure adjustment to accommodate varying ambient lighting conditions. For nighttime monitoring, supplementary LED illumination was installed to ensure adequate image quality during low-light periods. The imaging system operated continuously over a 24-hour cycle, capturing the full range of diurnal and nocturnal fish behaviors.

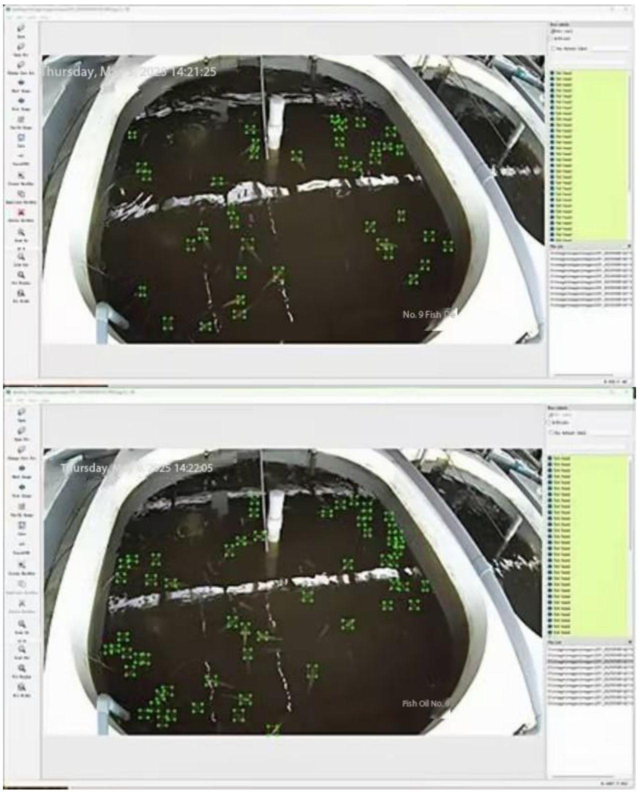

Figure 1. Overview of the image acquisition and annotation process. (a) Annotation example at timestamp 14:21:25; (b) annotation example at timestamp 14:22:05. (Overhead view of the cylindrical culture tank captured by the surveillance camera; example of bounding box annotations using LabelImg software, where green boxes indicate detected fish).

Dataset construction and annotation

(1) Data collection

Image acquisition was performed over multiple days, covering the complete 24-hour cycle (00:00-24:00) to capture behavioral variations across different time periods. The dataset incorporated images from both normal daylight conditions and nighttime periods with supplementary lighting, representing the diverse visual scenarios encountered in commercial RAS operations. Images were also collected from multiple tanks within the facility to increase sample diversity. A total of 13,600 images were collected for subsequent annotation and model training.

(2) Image annotation

Manual annotation was performed using the LabelImg software (version 1.8.6), an open-source graphical image annotation tool. Two behavioral categories were defined for annotation: (1) abnormal surface breathing (labeled as "gasp"), characterized by fish positioning at or near the water surface with their mouths oriented upward; (2) normal swimming behavior. Bounding boxes were drawn around the head and anterior body region of each fish exhibiting the target behaviors. Annotations were saved in YOLO format, containing normalized bounding box coordinates (center x, center y, width, height) and class labels for each detected object.

To ensure annotation quality and consistency, a subset of images was independently annotated by two trained personnel, and inter-annotator agreement was assessed. Discrepancies were resolved through discussion and consensus. The annotation process yielded over 1.2 million individual bounding box annotations across the entire dataset.

(3) Dataset partitioning

The annotated dataset was randomly divided into three subsets: a training set comprising 9,520 images (70%), a validation set comprising 2,720 images (20%), and a test set comprising 1,360 images (10%). This partitioning ratio ensured sufficient data for model training while reserving adequate samples for unbiased performance evaluation. Care was taken to ensure that images from the same time were not split across different subsets, thereby preventing data leakage and ensuring the independence of the test set.

YOLOv12 model architecture

YOLOv12, introduced by Tian, represents a significant architectural evolution in the YOLO series by adopting an attention-centric design paradigm [18]. Unlike its predecessors that relied primarily on convolutional neural network (CNN) backbones, YOLOv12 integrates attention mechanisms to enhance feature extraction capabilities while maintaining real-time inference speeds. This section describes the key architectural components of YOLOv12 employed in this study.

(1) Area attention (a2) module. The core innovation of YOLOv12 is the area attention module, which addresses the computational inefficiency of standard self-attention mechanisms. Traditional self-attention has quadratic complexity with respect to input size, making it impractical for high-resolution feature maps in real-time detection tasks. The A2 module partitions feature maps into non-overlapping areas and computes attention within each area, substantially reducing computational overhead while preserving the ability to capture long-range dependencies. This design enables YOLOv12 to efficiently process large receptive fields, which is particularly beneficial for detecting objects of varying sizes in complex aquaculture environments.

(2) Residual Efficient Layer Aggregation Networks (R-ELAN). YOLOv12 incorporates R-ELAN as its feature aggregation backbone, building upon the Efficient Layer Aggregation Networks (ELAN) introduced in previous YOLO versions. R-ELAN introduces two key improvements: (1) a block-level residual design with scaling techniques to stabilize training, especially for larger model variants; (2) a redesigned feature aggregation method that enhances gradient flow and feature reuse across network layers. These modifications improve the model's ability to learn discriminative features for distinguishing between normal swimming behavior and abnormal surface breathing patterns.

(3) Architectural optimizations. several additional optimizations distinguish YOLOv12 from conventional attention-based architectures:

FlashAttention integration: YOLOv12 incorporates FlashAttention to address memory access bottlenecks associated with attention computations, enabling efficient utilization of GPU memory bandwidth.

Simplified attention design: The model removes positional encoding commonly used in transformer architectures, resulting in a cleaner and faster implementation. Instead, a 7×7 separable convolution serves as a position perceiver to implicitly encode spatial information.

Optimized MLP ratios: The multi-layer perceptron (MLP) ratio is adjusted from the conventional value of 4.0 to approximately 1.2-2.0, better balancing computational resources between attention and feed-forward layers.

Reduced block depth: The number of stacked attention blocks is reduced to facilitate optimization and prevent gradient degradation in deeper networks.

(4) Model variants

YOLOv12 is available in five model scales: YOLOv12-N, YOLOv12-S, YOLOv12-M, YOLOv12-L, and YOLOv12-X, offering flexibility to balance detection accuracy against computational requirements. In this study, we employed the YOLOv12-S variant, which provides an appropriate trade-off between detection performance and inference speed suitable for real-time aquaculture monitoring applications.

Training configuration

(1) Hardware and software environment

All experiments were conducted on a workstation equipped with an Intel Core i9-12900K processor, 32 GB DDR4 RAM, and an NVIDIA GeForce RTX 3070 graphics card with 8 GB VRAM. The software environment consisted of Windows 11 operating system, Python 3.11, and PyTorch 1.13 deep learning framework. CUDA 12.4 was utilized to enable GPU-accelerated training.

(2) Hyperparameter settings

The model was trained for 100 epochs with a batch size of 32. A learning rate warmup strategy was employed during the first 3 epochs, with the initial learning rate linearly increasing from 0.00333 to a peak value of 0.00980. Subsequently, a cosine annealing learning rate schedule was applied, gradually decreasing the learning rate to approximately 0.00812 by the end of training. This scheduling approach facilitates rapid initial convergence while enabling fine-grained parameter optimization in later training stages.

(3) Training procedure

Each training epoch consisted of forward propagation, loss computation, backpropagation, and parameter update steps. The model was optimized using a composite loss function comprising three components: bounding box regression loss, classification loss, and distribution focal loss. The validation set was evaluated at the end of each epoch to monitor model performance and detect potential overfitting. Model checkpoints were saved whenever validation performance improved, and the best-performing weights were retained for final evaluation on the test set.

(4) Data augmentation

Standard data augmentation techniques were applied during training to improve model generalization, including random horizontal flipping, mosaic augmentation, and photometric distortions (brightness, contrast, saturation, and hue adjustments). These augmentations helped the model learn invariant representations robust to the visual variations present in real-world aquaculture monitoring scenarios.

Evaluation metrics

Model performance was assessed using standard object detection evaluation metrics:

Precision (P) measures the proportion of true positive detections among all positive predictions, reflecting the model's ability to minimize false alarms:

$$\mathrm{P} = \frac{\mathrm{TP}}{\mathrm{TP} + \mathrm{FP}}$$

Where TP denotes true positives and FP denotes false positives.

Recall (R) measures the proportion of actual positive instances that are correctly detected, indicating the model's ability to identify all relevant targets:

$$\mathrm{R} = \frac{\mathrm{TP}}{\mathrm{TP} + \mathrm{FN}}$$

Where FN denotes false negatives.

F1-score provides a harmonic mean of precision and recall, offering a balanced measure of detection performance:

$$\mathrm{F1} = \frac{2 \times \mathrm{P} \times \mathrm{R}}{\mathrm{P} + \mathrm{R}}$$

Mean Average Precision (mAP) is computed as the area under the precision-recall curve, averaged across all object classes. Two mAP variants were reported: mAP@0.5, calculated at an Intersection over Union (IoU) threshold of 0.5, and mAP@0.5:0.95, averaged across IoU thresholds from 0.5 to 0.95 in increments of 0.05. The latter metric provides a more comprehensive assessment of localization accuracy across varying detection stringencies.

Results

Dataset characteristics

The constructed dataset included 13,600 images of fish behavior in commercial recirculating aquaculture systems (RAS). It covered 24-hour periods with natural daytime light and LED nighttime lighting, as well as multiple tanks with varying water turbidity to reflect real-world aquaculture visual diversity.

Statistical analysis of annotations showed two behavioral categories: abnormal surface breathing (“gasp”) (the majority) and dead fish (“dead”) (Figure 2a). Bounding box analysis (Figure 2b) indicated most annotations were small, with normalized widths and heights mainly between 0.01 and 0.06, due to the overhead camera angle and the small apparent size of fish heads at the water surface. Annotation centers were distributed across the entire tank, with higher concentrations in the central culture area (Figure 2c), confirming the dataset represented spatial variability of fish positions. Joint distribution analysis (Figure 2d) further revealed relationships between bounding box parameters and geometric characteristics of detection targets.

Further joint distribution analysis of bounding box parameters (Figure 3) showed annotation centers (x, y) were widely distributed, with a bimodal y-axis distribution matching preferred fish location. Most bounding boxes had normalized dimensions between 0.01 and 0.03, reflecting the overhead perspective and limited exposed fish head area during surface breathing. The x-y scatter plot confirmed widespread distribution with higher central density where fish activity peaked. Correlation plots showed no strong dependencies between position and size parameters, indicating consistent target size across the camera's field of view.

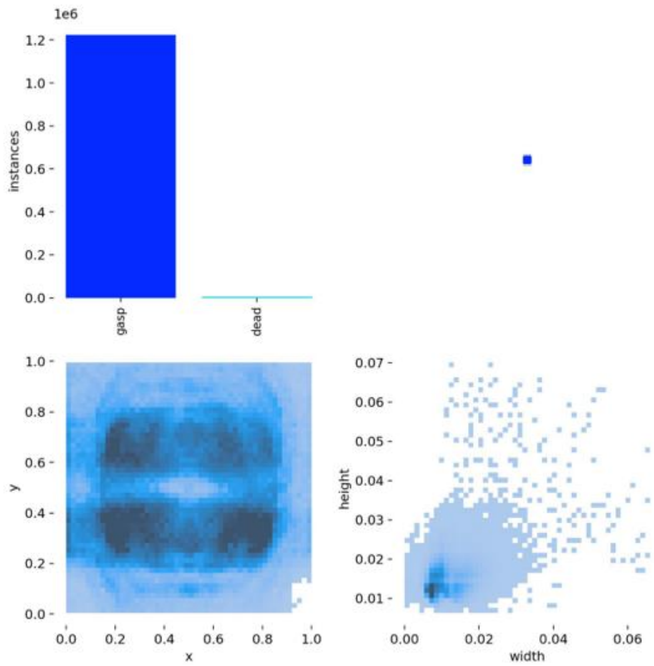

Figure 2. Statistical distribution of the dataset. (a) Class distribution showing the number of instances for each category; (b) Scatter plot of bounding box dimensions (width × height); (c) Spatial distribution of annotation centers; (d) Joint distribution of bounding box parameters.

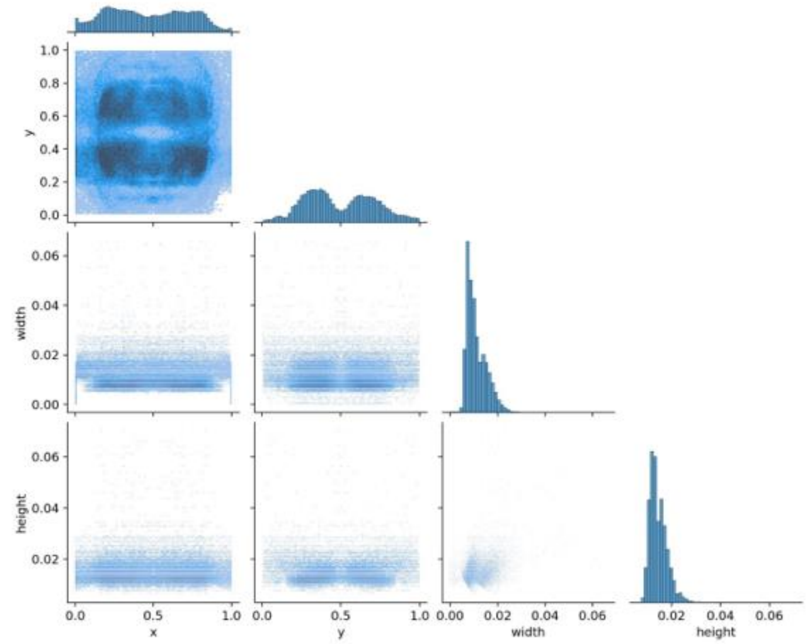

Figure 3. Joint distribution analysis of bounding box parameters in the annotated dataset. The diagonal panels display histograms showing the distribution of individual parameters: horizontal center position (x), vertical center position (y), normalized width, and normalized height. Off-diagonal panels present pairwise scatter plots illustrating correlations between parameters. The x-y density plot (top-left) reveals the spatial distribution of annotated fish across the tank area, with darker regions indicating higher annotation density.

Training process analysis

The YOLOv12-S model was trained for 100 epochs, and the training dynamics were monitored through loss curves for both training and validation sets (Figure 4). training and validation across all task-specific loss metrics. The training process exhibited three distinct phases characteristic of successful deep learning optimization.

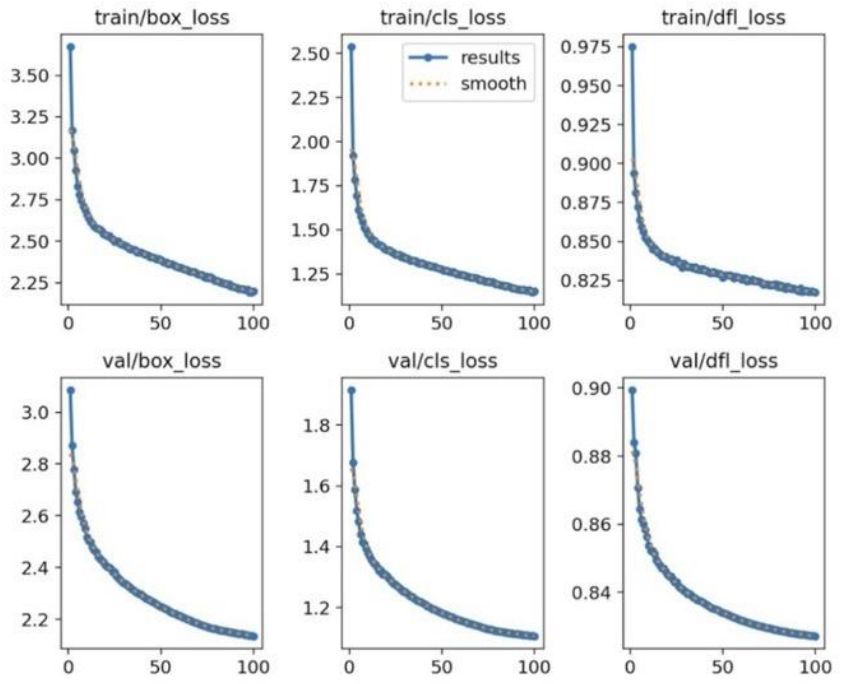

Figure 4. Training and validation loss curves over 100 epochs. Top row: training losses (box regression, classification, distribution focal loss); bottom row: corresponding validation losses.

During the initial phase (epochs 1-20), all loss components decreased rapidly, indicating that the model was effectively learning the fundamental visual features associated with fish surface breathing behavior. The classification loss showed the most pronounced reduction (approximately 41.7% decrease), demonstrating rapid improvement in the model's ability to discriminate between abnormal surface breathing and normal swimming behavior. The bounding box regression loss and distribution focal loss also decreased substantially during this phase.

In the intermediate phase (epochs 21-80), the rate of loss reduction slowed considerably as the model transitioned from coarse feature learning to fine-grained parameter optimization. Importantly, the training and validation loss curves maintained consistent downward trends without significant divergence, suggesting that the model was not overfitting to the training data. This parallel behavior between training and validation metrics indicated good generalization capability.

During the final phase (epochs 81-100), loss values stabilized and approached convergence. At epoch 100, the training bounding box loss stabilized at approximately 1.75, while the validation bounding box loss stabilized at approximately 1.88. The small difference between training and validation losses (less than 0.1) confirmed that the model had reached a near-optimal state with stable generalization performance. The best model weights were obtained at epoch 99, which achieved the optimal balance across all evaluation metrics.

Detection performance

The trained YOLOv12-S model was evaluated on the held-out test set comprising 1,360 images. Table 1 summarizes the detection performance metrics. The detailed statistics can be found in appendix A.

Table 1. Detection performance of YOLOv12-S on the test set.

Metric	Value (%)
Precision	84.78
Recall	69.42
F1-score	76.34
mAP@0.5	77.63
mAP@0.5:0.95	48.28

(1) Precision analysis

The model achieved a precision of 84.78%, indicating that the majority of positive predictions corresponded to true instances of abnormal surface breathing behavior. This high precision translates to a false positive rate of only 15.22%, which is critical for practical deployment where excessive false alarms would undermine system reliability and increase operational costs through unnecessary interventions.

(2) Recall analysis

The recall of 69.42% indicates that the model successfully detected approximately 70% of all actual abnormal surface breathing instances in the test set. While this represents effective coverage of most abnormal behavior events, the 30.58% miss rate suggests room for improvement. Analysis of false negative cases revealed that missed detections were primarily associated with: (1) fish exhibiting surface breathing behavior at the tank periphery where image resolution was lower; (2) instances where water surface reflections obscured fish features; and (3) cases where the exposed portion of the fish head was particularly small or partially occluded.

(3) F1-score analysis

The F1-score of 76.34% represents a balanced trade-off between precision and recall, indicating that the model achieves reasonable performance across both metrics simultaneously. This balance is particularly important for aquaculture monitoring applications, where both false alarms (low precision) and missed detections (low recall) carry operational consequences.

(4) mAP analysis

The mAP@0.5 of 77.63% demonstrates strong detection performance under standard evaluation criteria, indicating that the model reliably localizes abnormal surface breathing behavior with adequate spatial accuracy. The precision-recall curve (Figure 5c) illustrates the relationship between precision and recall across different confidence thresholds, with the area under this curve corresponding to the reported mAP value.

The mAP@0.5:0.95 of 48.28% reflects performance across more stringent localization requirements. This lower value compared to mAP@0.5 indicates that while the model successfully identifies the general location of surface breathing fish, precise bounding box localization becomes more challenging under stricter IoU thresholds. This is attributable to the inherent difficulty of precisely delineating fish boundaries at the air-water interface, where visual features are often indistinct due to water surface disturbance and reflection.

(5) Confidence threshold analysis

The precision-confidence and recall-confidence curves (Figure 5a, 5b) reveal the model's behavior across different operating points. At the default confidence threshold, the model achieves the reported precision and recall values. The F1-confidence curve (Figure 5d) indicates that optimal F1 performance (0.75) is achieved at a confidence threshold of approximately 0.210, providing guidance for threshold selection in practical deployment scenarios.

(6) Class-specific performance

The precision-recall curve analysis revealed differential performance between categories. The "gasp" class (abnormal surface breathing) achieved an AP of 0.576 at IoU 0.5, while the "dead" class achieved a higher AP of 0.976. The superior performance on the "dead" class is attributed to the more distinctive and static visual features of deceased fish compared to the dynamic and variable appearance of fish engaged in surface breathing behavior.

Qualitative results

Visual inspection of detection results demonstrated that the YOLOv12-S model successfully identified abnormal surface breathing behavior across diverse imaging conditions (Figure 5). Under daytime conditions with natural lighting, the model accurately detected fish positioned at the water surface with high confidence scores. The model also maintained detection capability under nighttime conditions with supplementary lighting, although slightly reduced confidence scores were observed in some cases due to altered color characteristics and increased noise levels.

The model demonstrated robustness to common visual challenges in aquaculture environments, including water surface reflections, varying turbidity levels, and partial occlusions caused by overlapping fish. However, detection failures were observed in cases of extreme reflection glare and when fish exhibited only minimal exposure above the water surface.

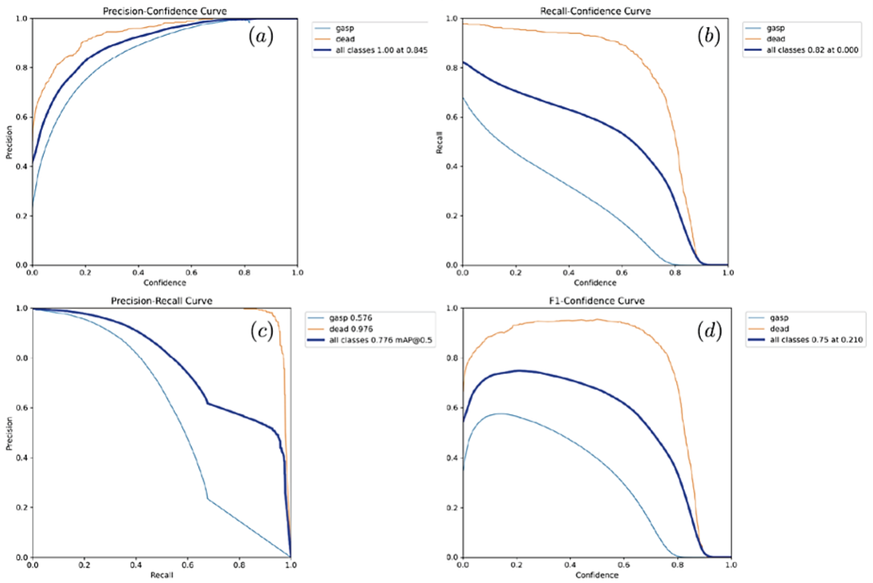

Figure 5. Performance evaluation curves on the test set. (a) Precision-confidence curve; (b) recall-confidence curve; (c) precision-recall curve; (d) F1-confidence curve.

Discussion

Performance analysis

The YOLOv12-S model demonstrated promising performance for detecting abnormal surface breathing behavior in largemouth bass under commercial RAS conditions. The achieved precision of 84.78% is particularly noteworthy for practical aquaculture applications, as it indicates that the vast majority of system alerts correspond to genuine behavioral anomalies. In intensive aquaculture operations, false alarms can lead to unnecessary equipment activation (such as emergency aeration systems), resulting in increased energy consumption and operational costs. The low false positive rate achieved by our model (15.22%) effectively addresses this concern, making it suitable for integration into automated early warning systems.

The model's ability to distinguish between abnormal surface breathing and normal swimming behavior can be attributed to the attention-centric architecture of YOLOv12. The Area Attention module enables the model to capture contextual information across larger receptive fields, facilitating recognition of the characteristic postural features associated with surface breathing, such as the upward orientation of the fish head and positioning at the air-water interface. These findings align with recent studies demonstrating the advantages of attention mechanisms for fine-grained behavioral recognition tasks in aquaculture settings [19].

However, the recall of 69.42% indicates that approximately 30.00% of abnormal surface breathing instances remained undetected. This limitation is primarily attributable to three factors identified through error analysis. First, small target size poses a significant challenge, as fish exhibiting surface breathing behavior often expose only a small portion of their head above water, resulting in bounding boxes with limited pixel information for feature extraction. Second, water surface reflections and glare can obscure fish features, particularly under certain lighting angles during daytime conditions. Third, fish located at tank peripheries appear smaller due to the overhead camera geometry, reducing detection sensitivity in these regions.

The differential performance between mAP@0.5 (77.63%) and mAP@0.5:0.95 (48.28%) reveals that while the model reliably identifies the presence and approximate location of surface breathing behavior, precise bounding box localization remains challenging. This discrepancy is consistent with the inherent difficulty of delineating exact boundaries at the dynamic air-water interface, where fish contours are frequently distorted by water surface tension and movement.

Practical implications

The proposed detection system offers several practical advantages for RAS facility management. Continuous automated monitoring addresses the fundamental limitations of manual observation, which is inherently intermittent, subjective, and labor-intensive. By enabling 24-hour surveillance with consistent detection criteria, the system can identify early signs of hypoxia that might otherwise be missed during periods without human oversight, particularly during nighttime hours when staffing is typically reduced.

From an economic perspective, early detection of abnormal surface breathing behavior provides aquaculture operators with critical response time to implement corrective measures before hypoxia escalates to lethal levels. Interventions such as activating supplementary aeration, reducing feeding rates, or adjusting water exchange can be initiated promptly upon system alert, potentially preventing mass mortality events that cause substantial financial losses. Furthermore, the ability to distinguish abnormal behavior from normal swimming reduces unnecessary interventions, optimizing resource utilization and minimizing operational disruptions.

The real-time inference capability of YOLOv12 makes it well-suited for deployment in production environments where immediate response is essential. The model's compatibility with standard surveillance camera infrastructure means that existing monitoring systems can potentially be upgraded with intelligent detection capabilities without extensive hardware modifications.

Limitations

Several limitations of the current study warrant consideration. First, the dataset was collected from a single facility using largemouth bass as the sole experimental species. The generalizability of the trained model to other fish species, which may exhibit different surface breathing postures, remains to be validated. Second, the dataset size of 13,600 images, while substantial, may not fully capture the complete range of visual variations encountered across different RAS facilities with varying tank geometries, lighting configurations, and water quality conditions.

Third, the current study focused exclusively on detection without incorporating temporal tracking of individual fish behavior. Integration of object tracking algorithms could enable more sophisticated behavioral analysis, such as quantifying the duration and frequency of surface breathing episodes for individual fish, which may provide additional diagnostic value for assessing hypoxia severity.

Finally, while the model achieved satisfactory precision, the recall rate leaves room for improvement, particularly for detecting subtle or partially visible surface breathing instances. The current camera resolution and mounting height represent practical constraints that may limit detection of small targets at the water surface.

Future directions

Several avenues for future research emerge from this study. First, hardware improvements including higher-resolution cameras and optimized mounting positions could enhance image quality and reduce the small target detection challenge. Additionally, polarizing filters or alternative lighting arrangements may help mitigate water surface reflection interference.

Second, model architecture refinements specifically targeting small object detection could improve recall performance. Techniques such as feature pyramid network enhancements, attention mechanisms focused on small-scale features, or multi-scale training strategies may prove beneficial for this application.

Third, expanding the dataset to include multiple fish species, facility types, and environmental conditions would improve model robustness and generalizability. Transfer learning approaches could facilitate adaptation to new species with limited additional training data.

Fourth, integration with complementary sensing modalities, such as dissolved oxygen sensors and water quality monitors, could enable multi-modal fusion approaches that combine visual behavioral indicators with physicochemical measurements for more reliable hypoxia prediction.

Conclusion

This study develops and evaluates a YOLOv12-based detection system for recognizing abnormal surface breathing behavior in farmed largemouth bass under commercial recirculating aquaculture conditions. A comprehensive dataset of 13,600 images is constructed, covering diverse lighting conditions and time periods representative of practical RAS operations. The YOLOv12-S model, featuring attention-centric architecture with Area Attention modules and R-ELAN feature aggregation, is trained and optimized for this specific detection task.

Experimental results demonstrate that the proposed approach achieve a precision of 84.78%, recall of 69.42%, F1-score of 76.34%, and mAP@0.5 of 77.63% on the independent test set. These performance metrics indicate that the model can effectively distinguish abnormal surface breathing from normal swimming behavior with high reliability, meeting the low false-alarm requirements essential for practical aquaculture deployment.

The primary contributions of this work include: (1) establishment of a labeled dataset for fish surface breathing behavior detection in RAS environments; (2) successful application of the latest attention-centric YOLOv12 architecture to aquaculture behavioral monitoring; (3) systematic evaluation demonstrating the feasibility of automated detection under realistic commercial conditions.

While the current system demonstrates promising performance, future work should focus on improving recall through hardware upgrades and model refinements, validating generalizability across multiple species and facilities, and integrating temporal tracking for comprehensive behavioral analysis. The proposed approach provides a technical foundation for intelligent early warning systems in precision aquaculture, contributing to improved fish welfare, reduced economic losses, and enhanced sustainability of intensive aquaculture operations.

Funding

This work was not supported by any funds.

Acknowledgements

The author would like to show sincere thanks to those techniques who have contributed to this research.

Conflicts of Interest

The author declares no conflict of interest.

References

[1] Kang, B., Huang, X., Li, J., Liu, M., Guo, L., Han, C. C. (2017) Inland fisheries in China: past, present, and future. *Reviews in Fisheries Science & Aquaculture*, 25(4), 270-285.

[2] Espinal, C. A., Matulić, D. (2019) Recirculating aquaculture technologies. *Aquaponics Food Production Systems*, 1, 35-76.

[3] Chen, W., Gao, S. (2023) Current status of industrialized aquaculture in China: a review. *Environmental Science and Pollution Research*, 30(12), 32278-32287.

[4] Wang, H., Zhang, S., Zhao, S., Lu, J., Wang, Y., Li, D., Zhao, R. (2022) Fast detection of cannibalism behavior of juvenile fish based on deep learning. *Computers and Electronics in Agriculture*, 198, 107033.

[5] Domenici, P., Steffensen, J. F., Marras, S. (2017) The effect of hypoxia on fish schooling. *Philosophical Transactions of the Royal Society B: Biological Sciences*, 372(1727), 20160236.

[6] Mandic, M., Flear, K., Qiu, P., Pan, Y. K., Perry, S. F., Gilmour, K. M. (2022) Aquatic surface respiration improves survival during hypoxia in zebrafish (Danio rerio) lacking hypoxia-inducible factor 1-α. *Proceedings of the Royal Society B*, 289(1966), 20211863.

[7] Fang, J., Zhang, X., Chen, Y., Zhao, Y., (2023). Hypoxia-induced physiological responses in fish: From organism to tissue to molecular levels. *Ecotoxicology and Environmental Safety*, 267, 115632.

[8] Li, D., Wang, G., Du, L., Zheng, Y., Wang, Z. (2022) Recent advances in intelligent recognition methods for fish stress behavior. *Aquacultural Engineering*, 96, 102222.

[9] An, D., Hao, J., Wei, Y., Wang, Y., Yu, X. (2021) Application of computer vision in fish intelligent feeding system - a review. *Aquaculture Research*, 52(2), 423-437.

[10] Li, D., Du, L. (2022) Recent advances of deep learning algorithms for aquacultural machine vision systems with emphasis on fish. *Artificial Intelligence Review*, 55(5), 4077-4116.

[11] Sapkota, R., Flores-Calero, M., Qureshi, R., Badgujar, C., Nepal, U., Poulose, A., Karkee, M. (2025) YOLO advances to its genesis: a decadal and comprehensive review of the You Only Look Once (YOLO) series. *Artificial Intelligence Review*, 58(9), 274.

[12] Al Muksit, A., Hasan, F., Emon, M. F. H. B., Haque, M. R., Anwary, A. R., Shatabda, S. (2022) YOLO-Fish: a robust fish detection model to detect fish in realistic underwater environment. *Ecological Informatics*, 72, 101847.

[13] Wang, H., Zhang, S., Zhao, S., Wang, Q., Li, D., Zhao, R. (2022) Real-time detection and tracking of fish abnormal behavior based on

improved YOLOV5 and SiamRPN++. *Computers and Electronics in Agriculture*, 192, 106512.

[14] Liu, M., Zhang, C., Lin, C. (2025) GAB-YOLO: A lightweight deep learning model for real-time detection of abnormal behaviors in juvenile greater amberjack fish. *Frontiers in Marine Science*, 12, 1574580.

[15] Wang, A., Chen, H., Liu, L., Chen, K., Lin, Z., Han, J. (2024) Yolov10: real-time end-to-end object detection. *Advances in Neural Information Processing Systems*, 37, 107984-108011.

[16] Yang, L., Liu, Y., Yu, H., Fang, X., Song, L., Li, D., Chen, Y. (2021) Computer vision models in intelligent aquaculture with emphasis on fish detection and behavior analysis: a review. *Archives of Computational Methods in Engineering*, 28(4), 1-32.

[17] Li, Y., Tan, H., Deng, Y., Zhou, D., Zhu, M. (2025) Hypoxia monitoring of fish in intensive aquaculture based on underwater multi-target tracking. *Computers and Electronics in Agriculture*, 232, 110127.

[18] Tian, Y., Ye, Q., Doermann, D. (2025) Yolov12: Attention-centric real-time object detectors. *arXiv Preprint arXiv:2502*, 12524.

[19] Wang, Z., Zhang, X., Su, Y., Li, W., Yin, X., Li, Z., Zhao, K. (2023) Abnormal behavior monitoring method of larimichthys crocea in recirculating aquaculture system based on computer vision. *Sensors*, 23(5), 2835.

Appendix

Table 1. Summary of core experimental parameters and data.

epoch	time	train/box_loss	train/cls_loss	train/dfl_loss	metrics/precision(B)	metrics/recall(B)	metrics/mAP50(B)
1	957.153	3.67376	2.53994	0.97516	0.43828	0.23070	0.24763
2	1851.260	3.16792	1.92005	0.89372	0.50606	0.39152	0.39447
3	2740.060	3.04823	1.78277	0.88110	0.55106	0.47066	0.48357
4	3628.520	2.92751	1.69240	0.87228	0.59971	0.49522	0.51682
5	4513.910	2.82980	1.61213	0.86381	0.58608	0.51661	0.52826
6	5397.190	2.78262	1.57442	0.85943	0.66000	0.55281	0.59458
7	6282.800	2.74773	1.54531	0.85622	0.68011	0.56352	0.61563
8	7167.620	2.71100	1.51178	0.85235	0.68134	0.57035	0.61978
9	8056.160	2.68835	1.49881	0.85127	0.67719	0.57641	0.62525
10	8944.530	2.65932	1.47627	0.84959	0.68403	0.59282	0.64036
11	9836.200	2.63880	1.46529	0.84780	0.71218	0.57750	0.64235
12	10724.000	2.61939	1.44448	0.84503	0.73615	0.59516	0.66172
13	11612.900	2.60928	1.44250	0.84562	0.73359	0.61406	0.67416
14	12501.600	2.59098	1.42927	0.84416	0.74801	0.59923	0.66116
15	13392.600	2.58021	1.41908	0.84259	0.73928	0.60522	0.67840
16	14284.500	2.57442	1.41515	0.84243	0.74569	0.61930	0.68359
17	15170.500	2.57140	1.41359	0.84034	0.73607	0.62121	0.68716
18	16060.000	2.56300	1.40578	0.84014	0.74846	0.61805	0.68934
19	16948.700	2.54408	1.39272	0.84045	0.73271	0.63716	0.68732
20	17839.600	2.53925	1.38652	0.83877	0.74684	0.62575	0.68970
21	18733.900	2.53236	1.38458	0.83855	0.76421	0.61647	0.69122
22	19625.000	2.53161	1.38076	0.83896	0.74103	0.63057	0.70050
23	20514.800	2.52040	1.37367	0.83714	0.75995	0.62467	0.70006
24	21403.900	2.51254	1.36927	0.83788	0.75373	0.63474	0.70012
25	22292.400	2.49894	1.35856	0.83807	0.78243	0.62865	0.70382
26	23179.600	2.50090	1.35930	0.83590	0.76692	0.63721	0.70533
27	24069.000	2.50021	1.35914	0.83577	0.76116	0.64371	0.70910
28	24959.500	2.48847	1.34699	0.83315	0.79707	0.63854	0.71361
29	25851.000	2.48171	1.34738	0.83570	0.76267	0.64597	0.71105
30	26744.100	2.47504	1.33983	0.83475	0.79453	0.63448	0.70883
31	27633.500	2.47154	1.33838	0.83368	0.77883	0.64287	0.71215
32	28529.600	2.46732	1.33573	0.83363	0.77516	0.63633	0.71561
33	29420.500	2.45494	1.32641	0.83346	0.81480	0.63145	0.71941
34	30312.600	2.45185	1.32633	0.83300	0.80814	0.63088	0.72021
35	31206.900	2.45280	1.32628	0.83345	0.80198	0.63425	0.72343
36	32101.000	2.44784	1.32042	0.83214	0.79112	0.64802	0.72547
37	32992.200	2.43453	1.31080	0.83227	0.78822	0.65736	0.73092
38	33881.700	2.43337	1.30828	0.83176	0.78930	0.64774	0.72807
39	34774.100	2.43365	1.31113	0.83251	0.78782	0.65538	0.72921

40	35664.100	2.42936	1.30733	0.83138	0.79278	0.65863	0.73480
41	36553.000	2.42315	1.30223	0.83118	0.78715	0.65487	0.73511
42	37441.000	2.41806	1.29856	0.83047	0.80711	0.65511	0.73448
43	38329.900	2.41735	1.29832	0.82992	0.80256	0.65756	0.73862
44	39225.100	2.40684	1.29183	0.82989	0.80562	0.66359	0.74067
45	40117.200	2.40510	1.29095	0.83040	0.80302	0.66302	0.74134
46	41006.700	2.40263	1.29045	0.82996	0.79874	0.66592	0.74232
47	41898.800	2.39725	1.28497	0.82926	0.79446	0.67157	0.74111
48	42790.900	2.39072	1.28096	0.82955	0.79186	0.68154	0.74740
49	43683.400	2.39378	1.27937	0.82875	0.81133	0.67580	0.75005
50	44575.200	2.38803	1.27671	0.82688	0.81388	0.67399	0.75164
51	45467.300	2.37809	1.26959	0.82818	0.81610	0.67144	0.75387
52	46357.600	2.37364	1.26931	0.82848	0.81572	0.67241	0.75275
53	47250.400	2.37500	1.26738	0.82845	0.80774	0.67691	0.75401
54	48142.200	2.36399	1.26131	0.82821	0.80538	0.67866	0.75508
55	49033.800	2.36151	1.25971	0.82767	0.78951	0.68622	0.75478
56	49926.200	2.36462	1.26133	0.82627	0.79487	0.68370	0.75589
57	50820.800	2.35686	1.25612	0.82738	0.80274	0.68354	0.75698
58	51714.200	2.34977	1.25008	0.82717	0.81625	0.67859	0.75781
59	52604.700	2.34476	1.24901	0.82672	0.80621	0.68730	0.75904
60	53498.900	2.34130	1.24513	0.82555	0.80748	0.68934	0.75951
61	54391.400	2.34076	1.24448	0.82642	0.80829	0.69019	0.75995
62	55285.200	2.33463	1.24018	0.82636	0.80836	0.68913	0.76078
63	56179.000	2.33032	1.23653	0.82445	0.80898	0.69132	0.76226
64	57074.000	2.32798	1.23649	0.82504	0.81193	0.68979	0.76369
65	57968.300	2.32196	1.23059	0.82473	0.80862	0.69053	0.76339
66	58860.600	2.31797	1.22855	0.82580	0.81155	0.69013	0.76377
67	59754.200	2.31866	1.22950	0.82435	0.80638	0.69341	0.76433
68	60646.200	2.31565	1.22763	0.82442	0.80682	0.69533	0.76519
69	61536.900	2.31080	1.22342	0.82444	0.80993	0.69506	0.76585
70	62429.500	2.30186	1.21655	0.82431	0.81291	0.69379	0.76613
71	63324.300	2.29843	1.21572	0.82341	0.82422	0.68884	0.76689
72	64222.500	2.29874	1.21410	0.82236	0.81825	0.69060	0.76766
73	65122.000	2.28836	1.20803	0.82245	0.82640	0.68905	0.76820
74	66020.700	2.28315	1.20660	0.82271	0.82403	0.68872	0.76935
75	66923.800	2.28835	1.20744	0.82180	0.81525	0.69363	0.76977
76	67822.600	2.27768	1.20095	0.82218	0.82226	0.69381	0.77052
77	68717.600	2.28487	1.20404	0.82186	0.82873	0.69051	0.77069
78	69614.600	2.27397	1.20020	0.82245	0.83046	0.69055	0.77107
79	70515.600	2.26527	1.19281	0.82253	0.83637	0.68835	0.77066
80	71415.600	2.26478	1.19271	0.82090	0.83362	0.68987	0.77087
81	72311.400	2.26008	1.18949	0.82206	0.83512	0.69130	0.77206
82	73206.700	2.25188	1.18491	0.82036	0.83423	0.69029	0.77139

83	74102.900	2.25138	1.18607	0.82097	0.83181	0.69411	0.77250
84	75002.400	2.24568	1.17921	0.81969	0.83365	0.69225	0.77190
85	75901.800	2.24577	1.18192	0.82114	0.83487	0.69258	0.77221
86	76800.800	2.24047	1.17788	0.82038	0.83766	0.69208	0.77245
87	77710.700	2.24122	1.17641	0.81949	0.83927	0.69494	0.77353
88	78612.000	2.22903	1.16897	0.81996	0.83386	0.69710	0.77368
89	79497.700	2.22946	1.16875	0.81918	0.83862	0.69561	0.77385
90	80374.300	2.22360	1.16477	0.81868	0.83864	0.69476	0.77400
91	81237.500	2.22036	1.16170	0.81823	0.84281	0.69271	0.77426
92	82096.600	2.21450	1.16280	0.81983	0.83782	0.69706	0.77458
93	82960.400	2.21517	1.15801	0.81779	0.84342	0.69451	0.77477
94	83824.200	2.21537	1.16165	0.81799	0.83992	0.69648	0.77509
95	84688.700	2.21112	1.15823	0.81849	0.84548	0.69298	0.77495
96	85557.200	2.20847	1.15535	0.81755	0.84571	0.69353	0.77551
97	86445.600	2.20979	1.15682	0.81767	0.84884	0.69250	0.77552
98	87421.200	2.19213	1.14652	0.81822	0.84826	0.69281	0.77564
99	88327.000	2.19286	1.14424	0.81766	0.84779	0.69421	0.77597
100	89175.000	2.19859	1.15267	0.81727	0.84597	0.69513	0.77628

Table 1. (Continued): Summary of core experimental parameters and data.

epoch	val/box_loss	val/cls_loss	val/dfl_loss	lr/pg0	lr/pg1	lr/pg2
1	3.08549	1.91509	0.89935	0.070005	0.003333	0.003333
2	2.87221	1.67607	0.88399	0.039939	0.006600	0.006600
3	2.77911	1.58836	0.88087	0.009807	0.009801	0.009801
4	2.69222	1.51745	0.87074	0.009703	0.009703	0.009703
5	2.65356	1.48279	0.86438	0.009604	0.009604	0.009604
6	2.61522	1.44016	0.86138	0.009505	0.009505	0.009505
7	2.59564	1.41582	0.86004	0.009406	0.009406	0.009406
8	2.57090	1.40879	0.85844	0.009307	0.009307	0.009307
9	2.54954	1.39451	0.85634	0.009208	0.009208	0.009208
10	2.51626	1.38005	0.85366	0.009109	0.009109	0.009109
11	2.50359	1.36930	0.85217	0.009010	0.009010	0.009010
12	2.49801	1.35710	0.85219	0.008911	0.008911	0.008911
13	2.47817	1.34544	0.85138	0.008812	0.008812	0.008812
14	2.46588	1.34102	0.84950	0.008713	0.008713	0.008713
15	2.45849	1.33228	0.84864	0.008614	0.008614	0.008614
16	2.44050	1.32054	0.84799	0.008515	0.008515	0.008515
17	2.43453	1.32150	0.84708	0.008416	0.008416	0.008416
18	2.42854	1.30935	0.84703	0.008317	0.008317	0.008317
19	2.42119	1.31057	0.84615	0.008218	0.008218	0.008218
20	2.41034	1.30552	0.84521	0.008119	0.008119	0.008119
21	2.40225	1.29712	0.84476	0.008020	0.008020	0.008020
22	2.40011	1.29072	0.84474	0.007921	0.007921	0.007921

epoch	val/box_loss	val/cls_loss	val/dfl_loss	lr/pg0	lr/pg1	lr/pg2
23	2.39276	1.28363	0.84381	0.007822	0.007822	0.007822
24	2.38310	1.27706	0.84302	0.007723	0.007723	0.007723
25	2.38133	1.27620	0.84296	0.007624	0.007624	0.007624
26	2.36519	1.26938	0.84182	0.007525	0.007525	0.007525
27	2.35902	1.26357	0.84120	0.007426	0.007426	0.007426
28	2.35351	1.25814	0.84107	0.007327	0.007327	0.007327
29	2.34411	1.25335	0.84044	0.007228	0.007228	0.007228
30	2.34009	1.25182	0.84028	0.007129	0.007129	0.007129
31	2.33589	1.24651	0.83954	0.007030	0.007030	0.007030
32	2.32939	1.24247	0.83953	0.006931	0.006931	0.006931
33	2.32587	1.23769	0.83899	0.006832	0.006832	0.006832
34	2.31876	1.23461	0.83848	0.006733	0.006733	0.006733
35	2.31362	1.22983	0.83830	0.006634	0.006634	0.006634
36	2.30815	1.22639	0.83790	0.006535	0.006535	0.006535
37	2.30186	1.22135	0.83761	0.006436	0.006436	0.006436
38	2.29850	1.22032	0.83745	0.006337	0.006337	0.006337
39	2.29733	1.21758	0.83715	0.006238	0.006238	0.006238
40	2.29169	1.21411	0.83675	0.006139	0.006139	0.006139
41	2.28677	1.21036	0.83640	0.006040	0.006040	0.006040
42	2.27979	1.20438	0.83614	0.005941	0.005941	0.005941
43	2.27745	1.20241	0.83575	0.005842	0.005842	0.005842
44	2.27206	1.19774	0.83542	0.005743	0.005743	0.005743
45	2.26755	1.19512	0.83526	0.005644	0.005644	0.005644
46	2.26568	1.19378	0.83506	0.005545	0.005545	0.005545
47	2.26043	1.19038	0.83487	0.005446	0.005446	0.005446
48	2.25740	1.18766	0.83457	0.005347	0.005347	0.005347
49	2.25245	1.18449	0.83425	0.005248	0.005248	0.005248
50	2.24892	1.18116	0.83398	0.005149	0.005149	0.005149
51	2.24468	1.17857	0.83379	0.005050	0.005050	0.005050
52	2.24185	1.17627	0.83360	0.004951	0.004951	0.004951
53	2.23773	1.17424	0.83339	0.004852	0.004852	0.004852
54	2.23370	1.17160	0.83311	0.004753	0.004753	0.004753
55	2.23009	1.16940	0.83286	0.004654	0.004654	0.004654
56	2.22601	1.16674	0.83269	0.004555	0.004555	0.004555
57	2.22287	1.16405	0.83247	0.004456	0.004456	0.004456
58	2.22024	1.16155	0.83222	0.004357	0.004357	0.004357
59	2.21559	1.15897	0.83197	0.004258	0.004258	0.004258
60	2.21269	1.15684	0.83178	0.004159	0.004159	0.004159
61	2.21041	1.15510	0.83161	0.004060	0.004060	0.004060
62	2.20713	1.15297	0.83148	0.003961	0.003961	0.003961
63	2.20388	1.15112	0.83130	0.003862	0.003862	0.003862
64	2.20027	1.14903	0.83109	0.003763	0.003763	0.003763

epoch	val/box_loss	val/cls_loss	val/dfl_loss	lr/pg0	lr/pg1	lr/pg2
65	2.19805	1.14726	0.83089	0.003664	0.003664	0.003664
66	2.19502	1.14547	0.83074	0.003565	0.003565	0.003565
67	2.19209	1.14335	0.83057	0.003466	0.003466	0.003466
68	2.18867	1.14146	0.83041	0.003367	0.003367	0.003367
69	2.18610	1.13981	0.83026	0.003268	0.003268	0.003268
70	2.18328	1.13817	0.83012	0.003169	0.003169	0.003169
71	2.18036	1.13610	0.83000	0.003070	0.003070	0.003070
72	2.17773	1.13418	0.82982	0.002971	0.002971	0.002971
73	2.17528	1.13242	0.82969	0.002872	0.002872	0.002872
74	2.17312	1.13083	0.82958	0.002773	0.002773	0.002773
75	2.17101	1.12943	0.82945	0.002674	0.002674	0.002674
76	2.16890	1.12791	0.82931	0.002575	0.002575	0.002575
77	2.16669	1.12622	0.82920	0.002476	0.002476	0.002476
78	2.16442	1.12482	0.82907	0.002377	0.002377	0.002377
79	2.16271	1.12365	0.82894	0.002278	0.002278	0.002278
80	2.16119	1.12268	0.82882	0.002179	0.002179	0.002179
81	2.15959	1.12171	0.82872	0.002080	0.002080	0.002080
82	2.15758	1.12060	0.82860	0.001981	0.001981	0.001981
83	2.15649	1.11974	0.82850	0.001882	0.001882	0.001882
84	2.15475	1.11880	0.82841	0.001783	0.001783	0.001783
85	2.15364	1.11788	0.82832	0.001684	0.001684	0.001684
86	2.15235	1.11700	0.82820	0.001585	0.001585	0.001585
87	2.15083	1.11602	0.82811	0.001486	0.001486	0.001486
88	2.14896	1.11494	0.82802	0.001387	0.001387	0.001387
89	2.14792	1.11411	0.82794	0.001288	0.001288	0.001288
90	2.14664	1.11330	0.82786	0.001189	0.001189	0.001189
91	2.14561	1.11250	0.82778	0.001090	0.001090	0.001090
92	2.14405	1.11152	0.82769	0.000991	0.000991	0.000991
93	2.14298	1.11081	0.82763	0.000892	0.000892	0.000892
94	2.14208	1.11001	0.82757	0.000793	0.000793	0.000793
95	2.14056	1.10933	0.82749	0.000694	0.000694	0.000694
96	2.13966	1.10867	0.82742	0.000595	0.000595	0.000595
97	2.13821	1.10794	0.82737	0.000496	0.000496	0.000496
98	2.13691	1.10730	0.82729	0.000397	0.000397	0.000397
99	2.13605	1.10669	0.82723	0.000298	0.000298	0.000298
100	2.13483	1.10608	0.82717	0.000199	0.000199	0.000199